Sensor and Simulation Notes

Note 239

1 January 1978

Sensors for Electromagnetic Pulse Measurements
Both Inside and Away from Nuclear Source Regions

Carl E. Baum
Edward L. Breen
John P. O'Neill

Air Force Weapons Laboratory
Kirtland AFB, NM 87117

Joseph C. Giles
Gary D. Sower

EG&G, Inc.
Albuquerque, NM 87108

Abstract

For measuring transient electromagnetic fields and related quantities one needs accurate broadband sensors with simple transfer functions. This paper summarizes the various sensor designs developed to achieve this in an optimal manner. Such sensors are designed for use either in a "free space" environment (such as in an EMP simulator or on a system under test in such a simulator) or in a nuclear source region which includes local source current and perhaps conductivity. There are now numerous designs which have been iterated for improvements over the last decade.

PL 96-1355

Sensor and Simulation Notes
Note 239

transient radiation, broadband sensors, electromagnetic pulse simulation,
source region radiation

Sensors for Electromagnetic Pulse Measurements Both Inside and Away from Nuclear Source Regions

CARL E. BAUM, MEMBER, IEEE, EDWARD L. BREEN, MEMBER, IEEE, JOSEPH C. GILES, MEMBER, IEEE,
JOHN O'NEILL, AND GARY D. SOWER, MEMBER, IEEE

Abstract—For measuring transient electromagnetic fields and related quantities, one needs accurate broadband sensors with simple transfer functions. The various sensor designs developed to achieve this in an optimal manner are summarized. Such sensors are designed for use either in a "free space" environment (such as in an EMP simulator or on a system under test in such a simulator) or in a nuclear source region that includes local source current and perhaps conductivity. There are now numerous designs which have been iterated for improvements over the last decade.

I. INTRODUCTION

IN MEASURING the nuclear electromagnetic pulse, one has to often deal with distributed electromagnetic quantities such as electric and magnetic fields, current densities, charge densities, and conductivity, as well as integral quantities such as voltage and current. As indicated in Fig. 1, there are four kinds of distributed quantities that are directly related by Maxwell's equations and constitutive equations [53]. This cyclic set of physical quantities is related to the nuclear source via the source current density J_c and the ionization source density S_e (electron-ion pairs per m^{3}s). It is these quantities, a combination of them, or simple transformations of them that one wishes to measure. The sensor problem is then basically how to measure these. (See the papers in this issue by Longmire concerning EMP environments, Higgins, Marin, and Lee concerning SGEMP, and Baum concerning EMP simulators.)

What then is a sensor? For purposes of this discussion, let us define a sensor as a special kind of antenna with the following properties.

1) It is an analog device which converts the electromagnetic quantity of interest to a voltage or current (in the circuit sense) at some terminal pair for driving a load impedance, usually a constant resistance appropriate to a transmission line (cable) terminated in its characteristic impedance.
2) It is passive.
3) It is a primary standard in the sense that for converting fields to volts and current, its sensitivity is well known in terms of its geometry; i.e., it is "calibratable by a ruler." The impedances of loading elements may be measured and trimmed. Viewed another way it is in principle as accurate as the standard field (voltage, etc.) in a calibration facility. (A few percent accuracy is typically easily attainable in this sense.)
4) It is designed to have a specific convenient sensitivity (e.g., 1.00×10^{-3} m^2) for its transfer function.
5) Its transfer function is designed to be simple across a wide frequency band. This may mean "flat" in the sense of volts per unit field or time derivative of field, or it may mean some other simple mathematical form that can be specified with a few constants (in which case more than one specific convenient sensitivity number is chosen).

For the measurement of local electric field and total current density quantities, we use an electric dipole sensor (dipole due to reciprocity between transmission and reception) as indicated in Fig. 2. The equivalent circuits are for the case
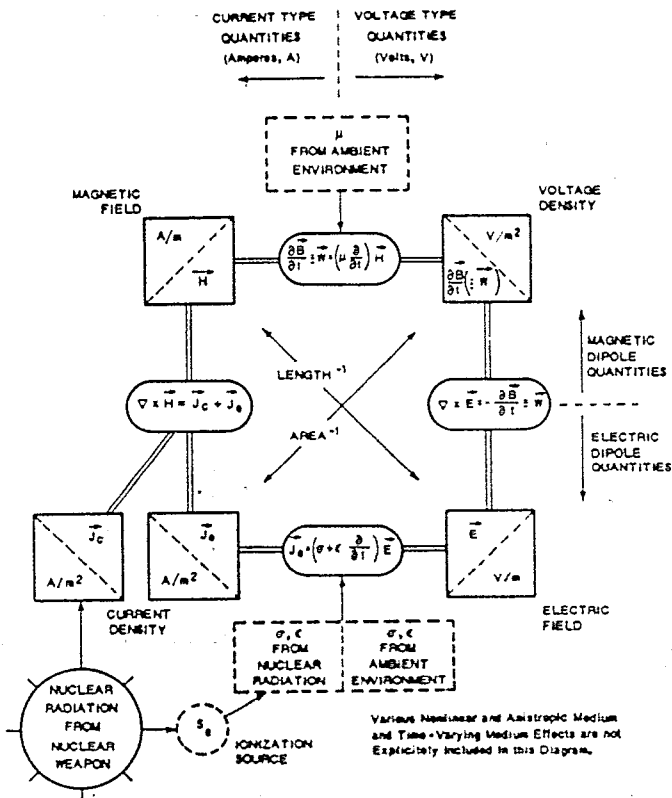
Fig. 1. Diagram of basic electromagnetic quantities for source region EMP environment and interaction.

Fig. 2. Electrically small electric dipole sensor in free space. (a) Thevenin equivalent circuit. (b) Norton equivalent circuit. (c) Electric dipole sensor.

where the sensor is electrically small. If the medium is conducting, then a conductance G appears in parallel with the capacitance C. In a nuclear source region in air, G is time dependent and a function of the electric field; there is a conduction as well as a displacement current density, and there is a source current density of high energy electrons. The Thevenin and Norton equivalent circuits correspond most conveniently to open circuit and short circuit conditions where the magnitude of the load impedance Z_c is large or small, respectively, compared to the magnitude of the source impedance $1/(\tilde{s}C)$, or better $1/(sC + G)$ where s is the complex frequency (Laplace transform variable with respect to time indicated by a tilde $\sim$ above a quantity). For open circuit purposes, the sensitivity is characterized by a constant equivalent length (or height) $l_{e_{eq}}$ (a vector) which samples the incident electric field in a dot product sense. For short circuit purposes, the sensitivity is characterized by an equivalent area $A_{e_{eq}}$ which samples the incident current density (displacement current density in free space) in a dot product sense with conventions as in Fig. 2. Note that $l_{e_{eq}}$, $A_{e_{eq}}$, and C are defined by the asymptotic form of the response in the electrically small sense. These parameters are not all independent but are related by

$$A_{e_{eq}} = \frac{C}{\epsilon_0} l_{e_{eq}} \qquad (1)$$

with ϵ_0 as the permittivity of free space (or other surrounding uniform isotropic medium) [22]. Note in Fig. 1 that open and short circuit for such a sensor correspond to two of the four basic types of quantities from Maxwell's equations.

For magnetic quantities we use a magnetic dipole sensor (a loop) as indicated in Fig. 3. The equivalent circuits for electrically small sensors are characterized by an inductance L (and perhaps some series resistance which is kept small), an equivalent area $A_{h_{eq}}$ for open circuit measurements for which $\partial B/\partial t$ is sampled (with units V/m^2 or voltage density), and an equivalent length $l_{h_{eq}}$ for short circuit measurements for which H is sampled. Open and short circuits correspond to the magnitude of Z_c (the load, usually resistive) large or small, respectively, compared to the magnitude of sL. These quantities are related by

$$A_{h_{eq}} = \frac{L}{\mu_0} l_{h_{eq}} \qquad (2)$$

where μ_o is the permeability of free space. Again, these parameters are defined by the asymptotic form of the response in the electrically small sense [22]. In Fig. 1, open and short circuit conditions correspond to the remaining two of the four basic types of quantities from Maxwell's equations.

An important question relating to these kinds of sensors is which type is best for a certain kind of application. Such questions are usually cast into an efficiency format in the sense of most output per unit input. Here one must recognize the broadband character of the measurement problem so that output should also include an appropriate bandwidth in its definition.
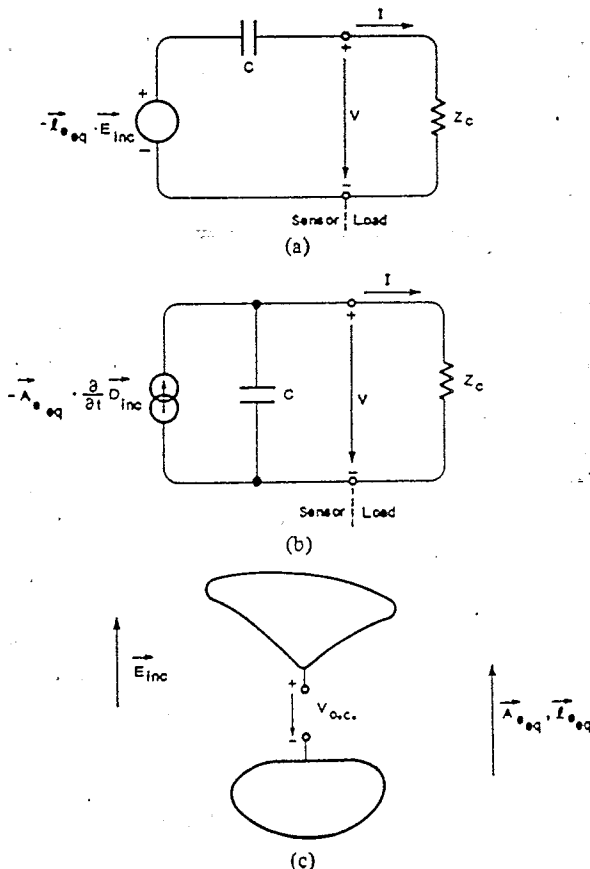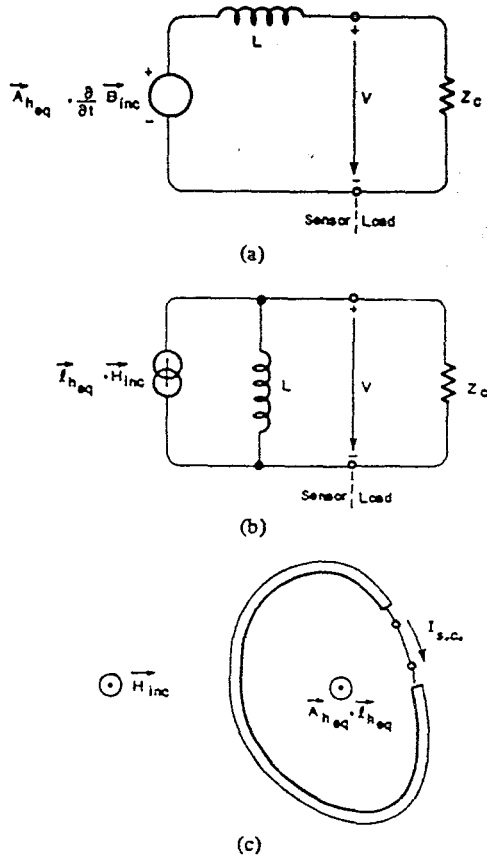
Fig. 3. Electrically small magnetic dipole sensor in free space. (a) Thevenin equivalent circuit. (b) Norton equivalent circuit. (c) Magnetic dipole sensor (loop).

One concept of historical and technical interest is that of equivalent volume that has the formulas [22], [34]

$$V_{e_{eq}} = \frac{\epsilon_0}{C} A_{e_{eq}} \cdot A_{e_{eq}} = \frac{C}{\epsilon_0} l_{e_{eq}} \cdot l_{e_{eq}} = A_{e_{eq}} \cdot l_{e_{eq}}$$

$$V_{h_{eq}} = \frac{\mu_0}{L} A_{h_{eq}} \cdot A_{h_{eq}} = \frac{L}{\mu_0} l_{h_{eq}} \cdot l_{h_{eq}} = A_{h_{eq}} \cdot l_{h_{eq}} \quad (3)$$

for electric and magnetic dipole sensors, respectively. The equivalent volume is based on the energy extracted from the incident field and delivered to the load. This equivalent volume can be divided by a geometrical volume to give a dimensionless efficiency. This geometrical volume might be a specified volume into which the sensor is to fit; the better sensor design has the better efficiency. This type of definition is appropriate for cases in which the sensor is electrically small at all frequencies of interest, the critical frequency $1/(Z_cC)$ and Z_c/L (for constant resistance Z_c) is within the electrically small regime, and the basic limitation on the sensor design is size.

Several of the sensor types discussed herein are not constrained directly by physical dimensions but by upper frequency response (ω_c or f_c which might be interpreted as a characteristic time t_c) for which the approximation of the response being proportional to the time derivative type of field quantity dotted into an equivalent area breaks down.

The sensor size can be made as large as possible to obtain sensitivity for a given bandwidth. As the sensor size is increased, the approximation of an electrically small sensor breaks down at the highest frequencies of interest. One defines then the characteristic frequency or time according to when the ideal dot product and derivative response is in error by some specified amount. The resulting figure of merit is found to be

$$\Lambda_e = \left(\frac{Z_c}{Z_0}\right)^{1/2} |A_{e_{eq}}| l_c^{-2} \qquad \Lambda_h = \left(\frac{Z_0}{Z_c}\right)^{1/2} |A_{h_{eq}}| l_c^{-2} \quad (4)$$

for electric and magnetic dipole sensors, respectively, where the wave impedance of free space is

$$Z_0 = \left(\frac{\mu_0}{\epsilon_0}\right)^{1/2} \quad (5)$$

and Z_c is the assumed frequency independent load resistance, typically the characteristic impedance of a transmission line. For this purpose, we have introduced a characteristic length (noting that the high-frequency limitation tends to be related to transit times on the structure) as

$$l_c = ct_c = \frac{c}{\omega_c} \quad (6)$$

with c being the speed of light, thus putting the bandwidth in length units. The figure of merit is of the form sensitivity times (bandwidth)^2, a quantity which is not a function of sensor size but only a function of the design, shape, and impedance loading distribution. The definition of this figure of merit is based on power delivered to the load Z_c which places electric and magnetic sensors on a common basis for comparison [52].

The various sensors in their free space designs can usually be mounted on ground planes by cutting them in half along an appropriate symmetry plane. The figures of merit for a given type of design are different in these two situations. In this paper we refer the figures of merit for each design type to their free space (full sensor) versions. Note that a particular sensor design in a ground plane version may have a different equivalent area and drive a different load impedance, although both are simply related to the free space versions.

Another common type of electromagnetic sensor is that used for measuring current or current density, specifically for measuring the time derivative of the current "through" the sensor via inductive coupling to the associated magnetic field [31]. An alternate scheme for measuring the current density involves a short-circuit electric dipole as in Fig. 2 [9]. However, this has significant limitations in nuclear source region applications.

The inductive current sensor is shown schematically in Fig. 4. It is characterized by a mutual inductance M relating the open circuit, (OC) voltage to the time derivative of the total current I_t (including displacement current, i.e., surface

$I_{t_{inc}} = \vec{A}_{t_{eq}} \cdot \vec{J}_{t_{inc}}$ For Measurement of Distributed Current Density

(a)

Sampling Loops to Integrate Around Perimeter - Parallel and/or Series Connections

$\vec{J}_t$ and I_t

$\vec{A}_{t_{eq}}$

Approximate Integration Pattern - Approximate Perimeter for Equivalent Area for Total Current Density
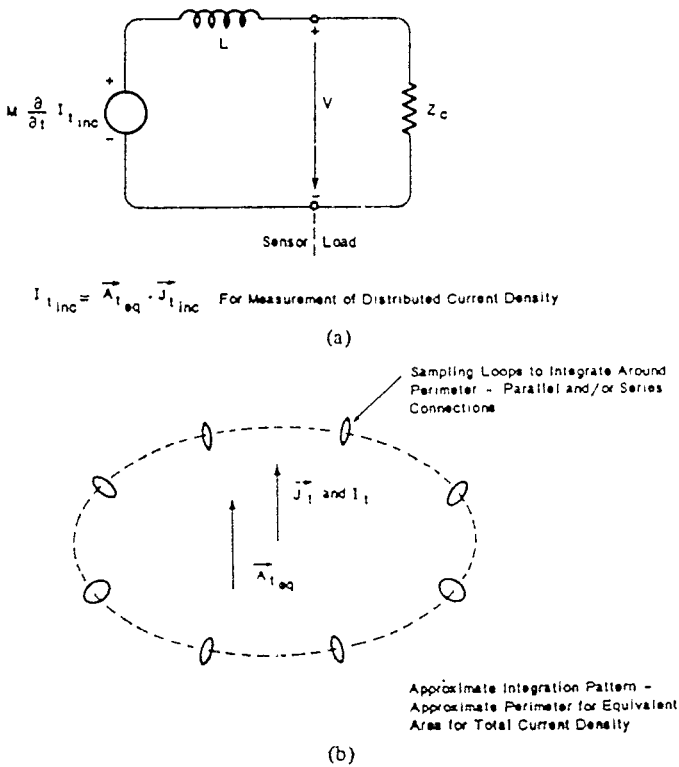
(b)

Fig. 4. Electrically small inductive current sensor in free space. (a) Norton equivalent circuit. (b) Inductive current sensor (multiple loops).

integral of $\epsilon \partial E/\partial t$). Inherent to the sensor design is the equality of the line integral of the magnetic field around an area to the surface integral of the total current density through the area. The basic relations are

$$V_{OC} = M \frac{\partial}{\partial t} I_{t_{inc}} \qquad I_{t_{inc}} = A_{t_{eq}} \cdot J_{t_{inc}}. \tag{7}$$

The latter equation is used in the case that the total current density is to be measured; $A_{t_{eq}}$ is the corresponding equivalent area. In this latter case there are two important sensitivity parameters, both of which must be considered for the accuracy of the sensor transfer function. Again, these parameters are defined by the asymptotic form of the response in the electrically small sense.

This type of sensor also has a self-inductance L which is in general not the same as M. One could modify the Thevenin equivalent circuit of Fig. 4 into a Norton form. However, this would bring the self-inductance L (which is in general not as accurately known as M) into the sensor sensitivity when operated in the short-circuit mode.

II. SENSORS FOR USE OUTSIDE OF NUCLEAR SOURCE REGIONS

In the simpler situation where there are no source currents in and around the sensor and the local medium is well behaved (typically free space), the problem is considerably simplified. This simpler situation allows one to pay more attention to accuracy details and bandwidth optimization. Several impor-
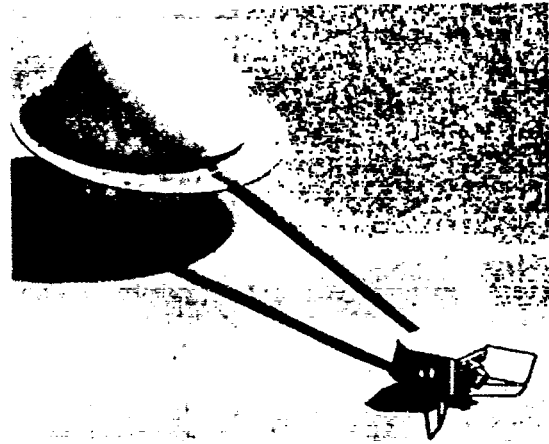

Fig. 5. HSD-2A(R) D-dot sensor.

tant kinds of sensor designs for electric and magnetic fields and current have been developed and used, and are discussed here.

A. D-Dot and Electric Field Sensors

1) D-Dot Sensors: The D-dot sensor is used to measure the time rate of change of electric flux density. The sensor's response is described by the Norton equivalent circuit of Fig. 2(b). The frequency domain response of the sensor is given by

$$\tilde{V}(s) = \frac{\epsilon s \tilde{E}_{inc}(s) \cdot A_{e_{eq}} Z_c}{1 + s Z_c C}, \tag{8}$$

and for frequencies where $\omega \ll 1/(Z_c C)$ the response can be simply expressed as

$$\tilde{V}(s) \cong \epsilon s \tilde{E}_{inc}(s) \cdot A_{e_{eq}} Z_c. \tag{9}$$

It is of primary importance that an accurate determination of sensor area can be made. For that reason, only sensor geometries with accurately calculable areas are used. Sensor capacitance as a design parameter need not be known so accurately, but it should be a low value as it shunts the load resistance and determines the high-frequency response.

a) Hollow spherical dipole (HSD): The HSD sensor design [38], [43], [51], [59], [84] uses the geometry of a sphere with a narrow slot around the equator. The slot is resistively loaded by the signal cables. The sensor shown in Fig. 5 is the HSD-2A(R). It consists of two hemispherical shells mounted on a ground plate. Signal current from each hemisphere flows to the ground plate through four equally spaced 200-Ω strip lines. The four strip lines from each hemisphere join at the center of the base of each hemisphere and then continue along a 50-Ω coaxial cable. The two 50-Ω coaxial cables are contained inside the output stem which extends radially out in the plane of the center plate to a twinaxial connector. The signals from the two hemispheres produce a differential signal which is then carried by standard 100-Ω twinaxial cable [10], [85]. The HSD-2A(R) is for use in making free space measurements. A single-ended version of the sensor for use on a conducting ground plane consists
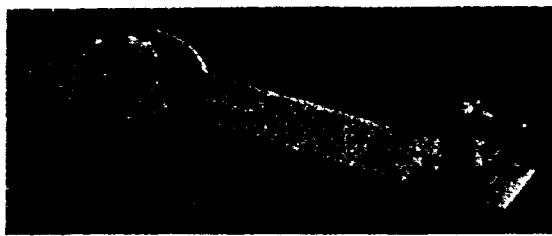
Fig. 6.　ACD–S1A(R) D-dot sensor.

of just one-half of the above sensor, and the signal is carried by a single 50-Ω coaxial cable. The sensitivity of the HSD sensor is expressed as an equivalent area. The area is shown to be $|A_{e_{eq}}| = 3\pi a^2$ where a is the sensor sphere radius [38], [43]. The Λ_{10-90} figure of merit for this sensor is 0.078. HSD sensors have been fabricated with equivalent areas of 0.1 and 0.01 m^2 in both differential and single-ended versions.

　　*b) Asymptotic conical dipole (ACD):* An improved sensor geometry from the standpoint of figure of merit is the ACD. The ACD sensor geometry is determined by a method described in [33], [84]. The particular shape used to date is derived from a line charge $\lambda(z)$ on the z axis given by

$$\lambda(z) = \begin{cases} \lambda_0, & \text{for } 0 < z < z_0 \\ -\lambda_0, & \text{for } 0 > z > -z_0 \\ 0, & \text{for } z = 0 \\ 0, & \text{for } |z| > z_0 \end{cases}$$

$$\lambda_0 > 0, \quad z_0 > 0. \tag{10}$$

The potential distribution for the above charge distribution is solved for the electrostatic equipotentials surrounding it. The surface of the sensor corresponds to a particular equipotential surface which approaches a 100-Ω cone at its base in its differential form. The ACD–S1A(R) sensor is shown in Fig. 6. The design details for this single-ended sensor are in [60]. It consists of the sensor element attached to a 50-Ω semirigid coaxial cable which passes within the ground plane to the coaxial connector. The sensor element is covered with a thin dielectric dome which provides weather protection and mechanical support. The sensor has an equivalent area of 1×10^{-4} m^2 and an upper frequency response > 7.6 GHz. Sensor element capacitance to ground is 1.16 pF. The Λ_{10-90} figure of merit is 0.23 (based on measurements on an inverse scale model (large)), which is comparable to the MGL B-dot sensors. The ACD sensors have been fabricated with equivalent areas of 10^{-3} and 10^{-4} m^2 in both differential and single-ended versions.

　　c) Flush plate dipole (FPD): The geometries of the HSD and ACD sensors cause electric field enhancement which is most pronounced at the top of the sensing element. The enhancement is three times for the HSD and larger for the ACD. The flush plate dipole minimizes field enhancement and chances for field distortion. The sensor geometry is shown in Fig. 7. It is basically a conducting disk centered in a circular aperture in a conducting ground plane [20], [39], [41], [69], [84]. The signal is taken from the sensor element at
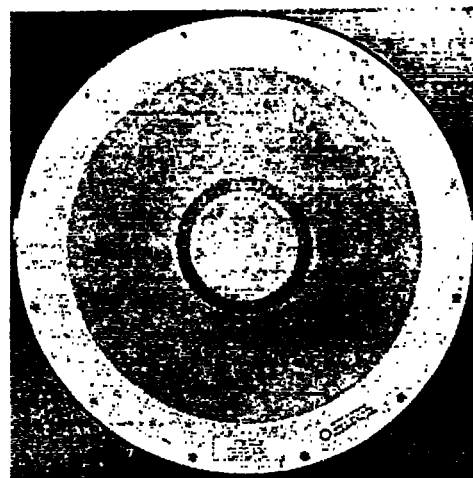
Fig. 7.　Flush plate dipole D-dot sensor.

four equally spaced points around its circumference by 200-Ω strip lines. The strip lines feed two 100-Ω coaxial cables which are paralleled into a 50-Ω connector. The flat surface of the sensor is covered by a thin piece of mylar which acts as a weather cover. The bottom side of the sensor is covered by a conducting pan to provide a consistent electrical environment as well as to provide protection. Resistive loops are positioned inside the cover to absorb energy below to the sensor element. The equivalent area of the FPD is derived in[41] in which the area is given as a normalized area $A = |A_{e_{eq}}|/(\pi ab)$ where a and b are the radii of the sensor element and the circular aperture, respectively. For the FPD-1A $a = 0.0508$ m, $b = 0.0635$ m, $A = 0.988$, and $A_{eq} = 0.01$ m^2. The normalized capacitance is calculated [41] for various disk and aperture radii, and for the dimensions of the FPD-1A that value is 6.8 pF. This value of capacitance along with the 50-Ω cable impedance would give a frequency response of 468 MHz. The presence of the mylar sheet covering the sensor, the disk support structure, and the bottom cover add an additional 1.2 pF and reduce the frequency response to approximately 390 MHz. The Λ_{10-90} figure of merit is 0.08 related to a differential configuration.

　　d) Conforming flush plate dipole (CFD): The CFD is designed for use on nonflat surfaces such as missile and aircraft skin where it is desired to measure surface charge density [20], [72], [84]. It consists of a conducting disk sensing element centered in a circular aperture in a conducting ground plane as is the previously discussed FPD. It differs from the FPD in that the volume below the sensing element is much reduced with a corresponding increase in capacitance. The sensor is fabricated from pliable materials which permit it to be mounted on cylindrical surfaces. The signal is taken from the sensing element to a small diameter 50-Ω cable that is sandwiched within the conducting surfaces of the sensor. The cable terminates on a 50-Ω connector. The equivalent area of the CFD-1A is 0.001 m^2, and it has a corner frequency of 106 MHz. The Λ_{10-90} figure of merit is 0.00053. Because of the low figure of merit, this sensor's use is limited to applications where the sensor must be mounted on nonflat surfaces. The CFD sensors have been fabricated with equivalent areas of 0.001 and 0.01 m^2.
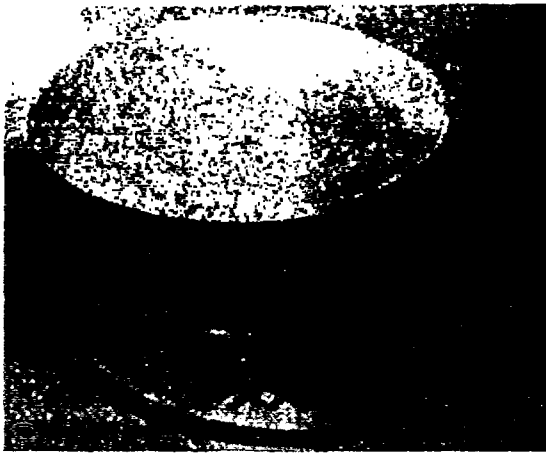
Fig. 8. PPD-1A(R) exploded view.

2) *Electric Field Sensors:* The common sensor for measuring electric field intensity is the parallel plate dipole (PPD). The PPD-1A(R) is shown in Fig. 8. This sensor [8], [36], [37], [45], [58], [84] is built in the form of a parallel plate capacitor. The conducting sensor plate is supported above a conducting baseplate by nylon spacers. The output signal is obtained from an attenuating resistor attached to the center of the top plate in series with a 50-Ω output cable in the sensor base which terminates in a coaxial connector. Sensor sensitivity is determined by the sensor plate equivalent height and the divider formed by the attenuating resistor and the output resistance. Sensor time constant is determined by the plate capacitance and the total resistance to ground. In order to attain a choice in sensitivity and time constant, the attenuating resistor is placed in an interchangeable resistor mount. The resistor mount has provisions for high-frequency compensation of the resistor's stray capacitance. Assuming proper compensation of the attenuating resistor, the frequency domain response of the sensor is given by

$$\tilde{V}_{o.c.}(s) = -\tilde{E}_{inc}(s) \cdot l_{e_{eq}} \frac{Z_c}{R + Z_c} \frac{sC(Z_c + R)}{sC(Z_c + R) + 1} \quad (11)$$

where $l_{e_{eq}}$ is the equivalent height of the sensor, R is the value of the attenuating resistor, and Z_c is the output cable impedance. The thickness of the base plate used with electric field sensors causes a field enhancement that must be considered in the height calculations [37]. The field enhancement above a base plate is approximated by the factor $(\pi/2)\xi_o$ where ξ_o is the ratio of the base plate thickness to radius for single-ended sensors and the ratio of plate thickness to diameter for differential sensors. Sensor capacitance [36] considers the effects of top plate thickness and fringing fields as well as the added capacitance from the nylon spacers. It is a desirable feature of the parallel plate dipole that a wave polarized normal to the plate and propagating across the plate is not perturbed by the sensor, and the frequency response for the sensor is determined only by the output circuitry. The rise time for the PPD sensor to this type of electric field is less than one nanosecond. The single-ended PPD sensor is the most commonly used, but a differential version has been built. It consists of a pair of circular parallel plates mounted on opposite sides of a
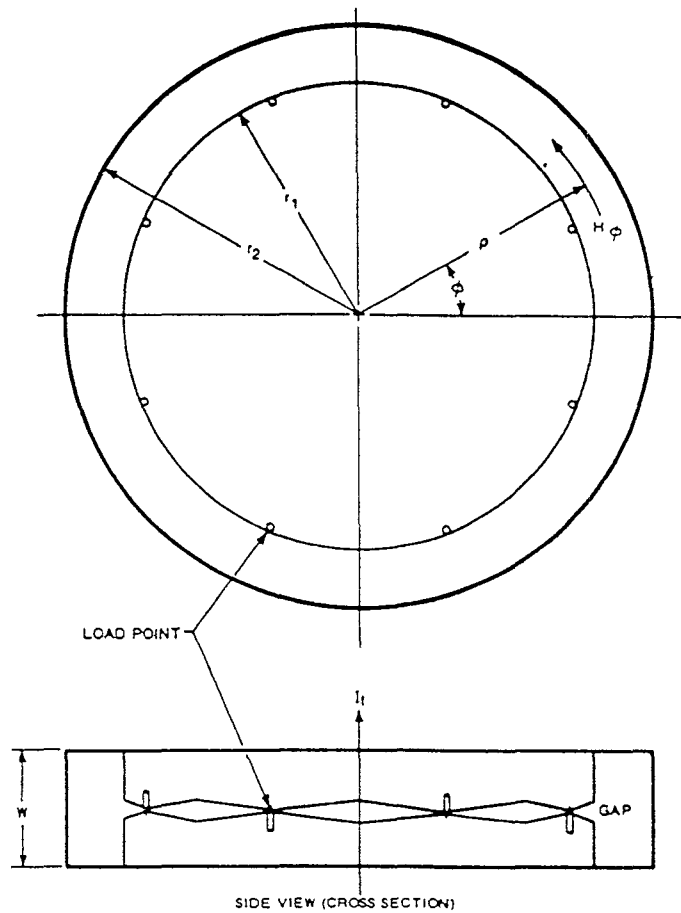

SIDE VIEW (CROSS SECTION)

Fig. 9. Typical CPM sensor geometry.

ground plate. The signals are taken from the plates in the same manner as for the PPD-1A(R). The 50-Ω cables from either side are joined in a twinaxial connector. The electric field sensors have been built with capacitances of one nF and 200 pF. The attenuating resistors are chosen to give time constants of 1, 10, and 100 microseconds. The sensor top plate is spaced 1 cm above the base plate. The accuracies of sensor height, capacitance, and resistor values are ±1 percent for each. The figure of merit rating does not apply for this sensor. The solid aluminum top plate can support undesirable resonances under certain excitations. This could be remedied by the use of a resistive top plate. ·

3) *Current Sensors:*

a) *Circular parallel mutual-inductance sensor (CPM):* This sensor is used to measure the time derivative of the total current through the aperture of the sensor. The CPM [31], [61], [65], [67], [84] is an inductive sensor of torodial shape as illustrated in Fig. 9. The loop turns are oriented to be sensitive to the component of the magnetic field H with respect to the measurement axis. This sensor has a cross section of width w, an inner radius r_1, and an outer radius r_2. The mutual inductance is

$$M = \frac{N\mu_r\mu_0 w \ln\left(\dfrac{r_2}{r_1}\right)}{2\pi} \quad (12)$$

where N is the effective number of turns, μ_r is the relative permeability of the sensor volume, and μ_o is the permeability of free space. For all CPM's developed to date, M is 10^{-8} H and $\mu_r = 1$. The CPM sensors have been built with aperture diameters of 0.1, 0.2, 0.5, 1 , and 2 m. The 10-90 response time of the sensors for on-axis current varies from 1 ns for the 0.1-m sensor to 3 ns for the 2-m sensor. The response time is further degraded by transit time effects for off-axis currents. The accuracy of the sensor is limited by manufacturing dimensional tolerances to ±1 percent.

  b) *I-dot One-Turn Insertion Unit (III):* The *I*-dot insertion unit is an inductive current sensor designed to respond to the time derivative of the current in the center conductor of a coaxial cable [31], [84]. The sensor is used by inserting it in series with a coaxial cable for the current measurement. The *I*-dot insertion unit operates on the same principles as the CPM current sensors. The basic form of the sensor is shown in Fig. 10. The sensor is constructed around the coaxial cable with the wall and sensing gap of the sensor forming an integral part of the outer conductor of the coaxial cable. The output signal is picked up by two 100-Ω cables whose center conductors cross the sensing gap at diametrically opposite points. The signals from the two 100-Ω cables are joined in parallel to a 50-Ω connector on the sensor wall. The III-1A current insertion unit has a mutual inductance of 5×10^{-9} H and a 10-90 rise time of less than 0.3 ns. It is designed for use with 1-5/8-in styroflex 100-Ω cable. Its accuracy is limited by manufacturing tolerances to ±3 percent.

B. Magnetic Field Sensors

  The transfer function of the magnetic field sensor of Fig. 3 is given by

$$\tilde{V}(s) = \frac{s\tilde{B}_{inc}(s) \cdot A_{h_{eq}}Z_c}{sL + Z_c}. \tag{13}$$

For frequencies where $\omega \ll Z_c/L$,

$$\tilde{V}(s) = s\tilde{B}_{inc}(s) \cdot A_{h_{eq}}. \tag{14}$$

For frequencies where $\omega \gg Z_c/L$,

$$\tilde{V}(s) = \frac{\tilde{B}_{inc}(s) \cdot A_{h_{eq}}Z_c}{L}. \tag{15}$$

Using the concept of equivalent length (2), the above (15) can be expressed as

$$\tilde{V}(s) = \tilde{H}_{inc}(s) \cdot l_{h_{eq}}Z_c. \tag{16}$$

  1) *Multigap Loop (MGL):* The MGL series of magnetic field sensors [25], [26], [57], [70], [73], [76], [77], [84] is used for high-frequency *B*-dot measurements. Signal distribution for these sensors is shown in Fig. 11. The sensor is built in the form of a right circular cylinder. The cylinder is formed from 1/16-in printed circuit board material which is etched to provide the gaps and the 200-Ω strip lines shown in Fig. 11. The sensor is divided into four quadrants by axial
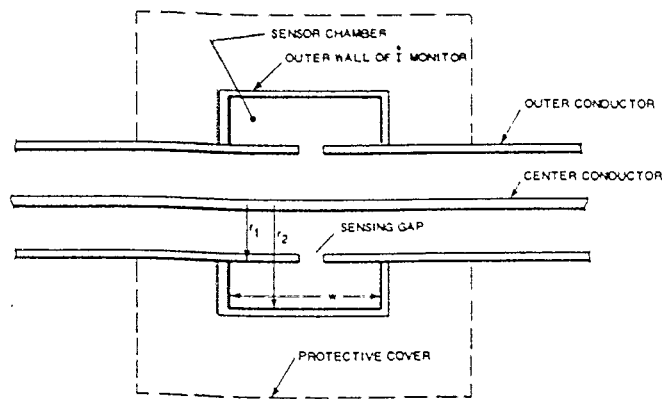

Fig. 10.   Insertion unit cross-sectional configuration.

shorting plates that connect to the cylinder midway between the gaps. The signals from quadrants one and three are combined to form one side of the differential output signal, and the signals from quadrants two and four combine to form the other. Combining the signals in this manner minimizes the *E*-field response. The gaps are formed with the proper angle to form a 200-Ω impedance which improves the sensor risetime. The cylindrical geometry of the MGL sensor permits an approximate determination [25] of the effects of the number of gaps, the cable impedance, the sensor length, and orientation of the gaps with respect to the magnetic field. The single-ended sensors are essentially one-half of the sensor described above except that they consist of two adjacent quadrants with signals connected in parallel. MGL sensors have been built with equivalent areas of 10^{-1}, 10^{-2}, 10^{-3}, 10^{-4}, and 10^{-5} m². Equivalent area is maintained to an accuracy of ±1 percent. The area accuracy considerations are discussed in [57]. The Λ_{10-90} figure of merit is 0.24.

  2) *One-Conductor, Many-Turn Loop (OML):* A single-gap half-cylinder loop with four-turn wiring [14], [84], and an equivalent area of one square meter is available for measurements requiring more sensitivity. This sensor, designated the OML-1A(A), operates as a derivative output device at frequencies below 3.5 MHz and has a rise time of about 100 ns. Fig. 12 shows the wiring diagram. Special triaxial cable with 25-Ω outer line and 50-Ω inner line is used. The gap voltage is picked off at four points and carried by the 25-Ω outer lines to two summing gaps in the 50-Ω internal lines. The two 50-Ω lines drive the 100-Ω differential output at the final gap in the cable. The four voltage pickoff points along the gap were selected experimentally to optimize frequency response.

  3) *Multiturn Loop (MTL):* The MTL-1 [24], [27], [46], [47], [66], [74] is a full-loop (free field) 50-turn sensor with an equivalent area of 10 m² and a *B*-dot upper frequency response of approximately 25 kHz. Above 25 kHz the sensor is self-integrating with its useful bandwidth extending to 3 MHz. Above this frequency, resonances within the complex signal distribution network perturb the output signal. The sensor has an equivalent length of 0.02 m and a self-inductance of 6.3×10^{-4} H. The MTL-1 design employs several special features to achieve the 3.5 MHz bandwidth [14]. It has four loop gap signal pickoffs and is wound in two identical 25 turn half-loops, each of which drives one side of the differ-
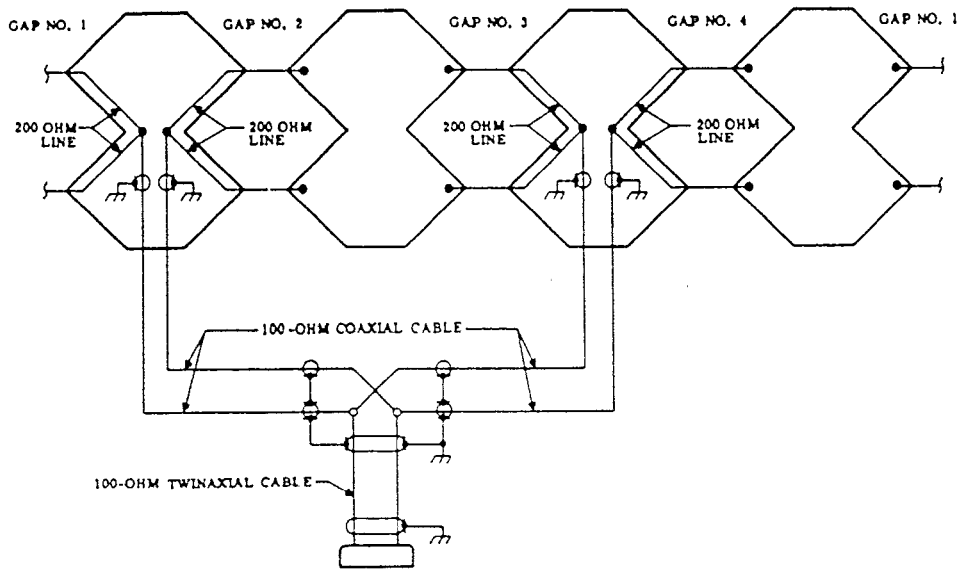
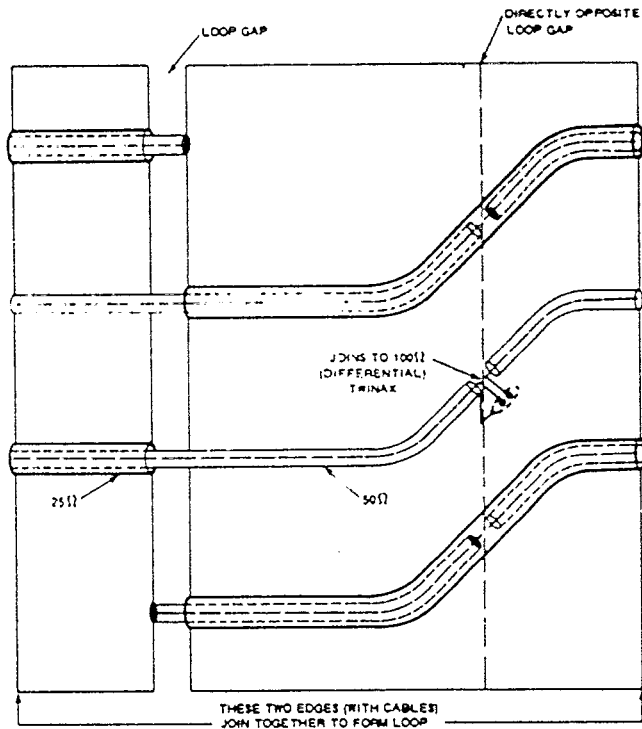Fig. 11. Multigap loop (MGL) *B*-dot sensors (signal distribution).

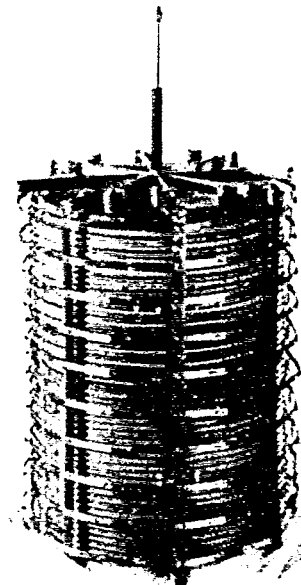Fig. 12. OML-1A(A) *B*-dot Loop Sensor (Expanded Diagram).

Fig. 13. MTL-1 sensor (coil with axial shorts and conducting shield in place).

ential output. Fig. 13 shows the sensor interior. A shield of resistively loaded loops can be seen on the outside of the coil. This shield is electrically connected to eight axial shorts which help break up resonances and keep out unwanted electric and magnetic field components. The 50-turn sensor loop is wound on a fiberglass coil form in a counterwound manner with a sequence of over and under crossovers on diametrically oppo-site sides of the coil. The signal is developed across the loop gaps and transmitted through 25-Ω outer part of a triaxial cable to the summing junction where they add and are trans-mitted to the sensor output connectors on a 50-Ω inner part of a triaxial cable. The two 50-Ω half-loop output cables then

combine to drive a 100-Ω differential output cable. The 25-Ω and 50-Ω signal cables are part of the sensor loop which is wound with 50/25-Ω triaxial cable. Midpoint grounds divide each half loop into two quarter loops. The midpoint ground structure consists of the sensor stem and connections to the loop structure at equipotential points, and do not affect the desired sensor response. They do, however, decrease the "electrical size" of the structure for undesired resonances and hence improve the high-frequency performance. Additional equipotential points are connected together to further improve the sensor response. Resistors are used in these "interwinding shorts" to dissipate the resonant energy. Final adjustments of the high-frequency response are made by adding a resistive shield around the outside of the coil to exclude the incident electric field at low frequencies. The quotient of equivalent volume divided by geometric volume is 1.3.
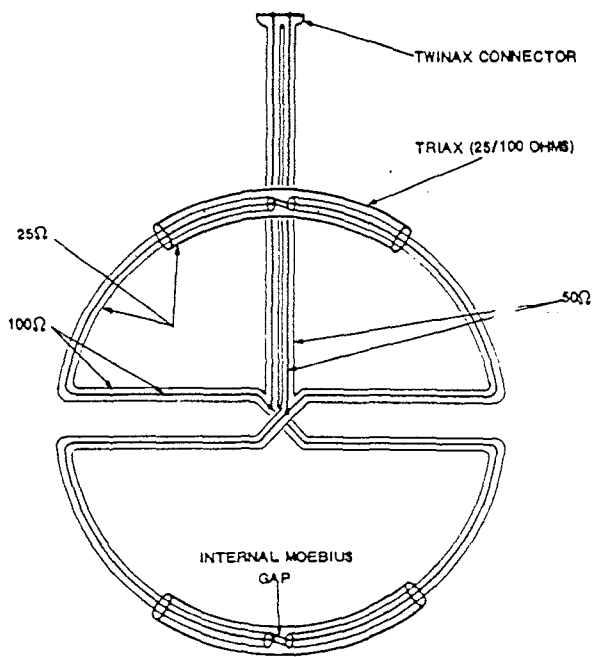
Fig. 14.   O3L-1 sensor (loop details for one of the three loops).

The MTL-2 has ten turns, an equivalent area of 10^{-2} m^2, an equivalent length of 10^{-2} m, a self-inductance of 1.25×10^{-6} H, and an upper frequency response of 12.6 MHz for B-dot operation. The quotient of equivalent volume divided by geometric volume is 0.56.

4) *Octahedral Three-Axis Loop (O3L) Sensor:* The O3L-1 sensor consists of three mutually orthogonal B-dot loops, and was designed for use as a trigger sensor for applications in which the angle of incidence and polarization of an incident wave are unknown [68]. Each loop as an equivalent area of 0.20 m^2, a self-inductance of 1.3×10^{-6} H, a rise time of 1 ns, and an upper frequency response for B-dot operation of 12 MHz. Each loop, shown schematically in Fig. 14, consists of four signal gaps, two moebius summing gaps, and two summing "tee" connections each driving one side of a differential output connector [14].

III. SENSORS FOR USE INSIDE A NUCLEAR SOURCE REGION

A. Introduction

The environment inside a nuclear source region is rather inhospitable for electromagnetic measurements [4], [53]. Referring to Fig. 1 we have a distributed source current density J_c which originates primarily from Compton scatter of γ rays and photoelectric scatter of X rays (the division not being precise). These processes occur in air (where present) as well as in the various materials of the sensor itself [11], [18].

Besides a source current density, we have conduction effects associated with the surrounding medium and perhaps in the sensor itself caused by the incident nuclear radiation [11], [17], [18], [19]. The impact of the air conductivity

(in an atmospheric environment) is fundamentally different for electric (capacitive-conductive) and magnetic (inductive) devices. Since the air conductivity is a nonlinear effect (because of the dependence of the electron mobility on the electric field), it is imperative that an electric type sensor not significantly distort the local electric field so as not to change the conductivity [11]. For a magnetic type sensor, the problem is somewhat different. Local changes in the air conductivity are not as significant; the magnetic field incident on the sensor is more governed by the currents in a volume of space with dimensions of the order of the radian wavelength (or skin depth) so that the local perturbations do not matter so much (at least for the lower frequencies) [18].

The problems of concern then include:

1) source currents in all materials present in the photon beam creating unwanted current and charge distributions and associated noise sources;
2) ionization of air, if present, which constrains electric sensor design to be nondistorting of the local electric field, and which loads the loop-gaps of magnetic sensors;
3) ionization of other dielectric materials (including surface tracking) which can load signals in the sensor and associated signal cables.

In reducing the deleterious effects in the nuclear source region various general guidelines are useful.

1) For sensors mounted on test objects, the sensor base should match the local surface of the test object both in material and shape.
2) Sensor cables should be made of low atomic number materials (both conductors and insulators with nearly matched atomic numbers). Differential signal outputs can also be used to reduce some of the noise signals.
3) Sensor cables should be removed from the radiation environment as soon as possible and shielded with high atomic number material (lead) to reduce the radiation, except very close to the cables where low atomic number materials can reduce the electron emission [54].
4) For magnetic sensors—

   In air they are encapsulated in dielectric with conductivity orders of magnitude lower than that of air under irradiation.

   In a vacuum they are made of sparse (grid) low atomic number materials to reduce electron emission.
5) For electric sensors—

   In air or vacuum they must negligibly distort the electric field in the immediate vicinity to not perturb (significantly) the current density, whether conduction current density as in air, or electron transport in vacuum as in SGEMP [15].

   In air or vacuum they are made of low atomic number materials and in a grid design to reduce electron emission.

Various designs of sensors for electric and magnetic fields and currents in nuclear source regions have been developed and used, and are discussed here.
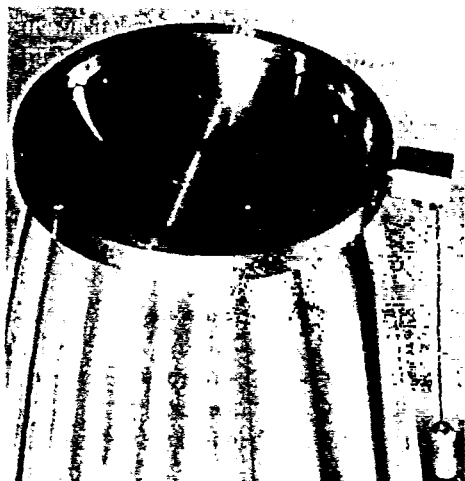
Fig. 15.   Parallel mesh dipole (PMD-1A) *E*-field sensor.

B. Electric Field Sensors

As discussed in the previous section, the most severe effect of a nuclear source environment on EMP measurements is that on the electric field sensor in air. The nuclear radiation displaces charge into and out of the sensor and the effects associated with air conductivity alter the characteristic response of the sensor. The parallel mesh dipole sensor (PMD-1) [1], [15], [82], [83] in Fig. 15 reduces the effect of the air conductivity by means of having its sensing element constructed of fine wires (0.0025 cm diameter in the *A* and *B* version, 0.0013 cm diameter in the *C* version) as opposed to the solid plate of a parallel plate dipole, so that most of the conduction current is allowed to flow around the dipole conductors instead of through them. This construction also minimizes the electrode mass while effectively keeping the electrical area nearly constant, thereby minimizing the Compton current from the air onto the electrode and from the electrode into the air. The mesh wire is aluminum or aluminum-magnesium alloy suspended from nylon thread 0.5 cm above the ground plane. In the quasi-static case, the wire grid lies on an equipotential plane so that the equivalent length of the sensor is also 0.5 cm. The output voltage of the *E*-field sensor is obtained by measuring, through a sensing resistor, the voltages across the capacitor/conductor formed by the wire mesh and the ground plane. The sensing resistor is in series with the terminated signal cable forming a resistive voltage divider [13]. The voltage across the capacitor will decay with a time constant determined by the sensor capacity (20 pF) and the sensing resistor except for local conductivity. This time constant must be long compared to measurement times of interest.

C. Magnetic Field Sensors

The maximum air conductivity limits the loop radius to the order of a skin depth or less at the highest frequency of interest. Below this frequency the air conductivity does not significantly enter into the loop response. Thus for such a loop the nonlinear and time varying character of the air conductivity is insignificant. However, sensor associated equipment such as cables in the air medium should generally be limited to the same dimensions to avoid magnetic field distortions which

may couple into the loop. It is possible to minimize the conductivity related effects by the use of insulators with the loop structure. Also, the cable impedance which loads the loop can be chosen, together with the loop inductance, to give a frequency response of the order of the skin depth limitation. The problem of air conductivity is eliminated in those sensors intended for use in nonvacuum environments by encapsulating the volume enclosing the sensing element with an epoxy resin which has a radiation induced conductivity of less than 10^{-5} $(S\ m^{-1})/(rad\ s^{-1})$. This material itself is a conductive medium under radiation but several orders of magnitude lower than sea level air. Those sensors intended strictly for use in vacuum have as little dielectric in them as possible.

Each segment of cable acts as a Compton diode in a gamma radiation field. Negative or positive charge is collected on the center conductor depending on the details of the charge transport. In addition, if the cable dielectric is hydrogenous (e.g., polyethylene), the center conductor will collect neutron scattered protons further complicating the picture. The signals produced by these radiation stimulated currents depend on the geometry of the sensor and the quality of the differencing techniques used.

The magnetic field sensors used in nuclear environments are all loop structures [3], [6], [7], [18], [19], [50], [55], [56], [75], [78], [80] with the signal cables wired in a moebius configuration designated as cylindrical moebius loop (CML) sensors. This greatly reduces the common mode radiation noise currents found in the split shield loop type of sensors and are made to have the same low differential radiation noise level (using symmetrical construction, etc.) as the split shield loop. A CML sensor can be shown to be a two-turn loop by tracking current flow from one twinaxial cable lead to the other (Fig. 16). At frequencies where the magnetic field does not penetrate the shield of the gap-loading cables, the sensor acts as a single-turn cylindrical loop with a resistive gap load given by the total terminating cable impedance. The four gap loading coaxial cables in the sensor are properly terminated at the point of coax-to-twinax junction as depicted in Fig. 16. A voltage *V* at the gap appears as a positive signal in one pair of 100-Ω gap-loading cables and as a negative signal in the other pair. The signal from the gap arrives at the coax-to-twinax junction at the same time from all four gap cables, which produces a differential mode signal across the balanced twinax. For a differential signal, the twinax may be considered to be two resistors each of a value of 50 Ω to ground that properly terminate the 50-Ω parallel combination of the two 100-Ω coaxial cables (from each side of the gap). For a given gap voltage, a signal voltage of twice the amplitude of the gap voltage appears at the balanced twinax output.

Six models of CML sensors have been designed and fabricated. They vary in equivalent area from 5 × 10^{-3} m² to 0.02 m², and have been built with encapsulation for use in air measurements and glyptol coated mesh materials for use in vacuum.

D. Current Sensors

Radiation hardened current sensors have been designed which are similar to the CPM series of *I*-dot probes [30],
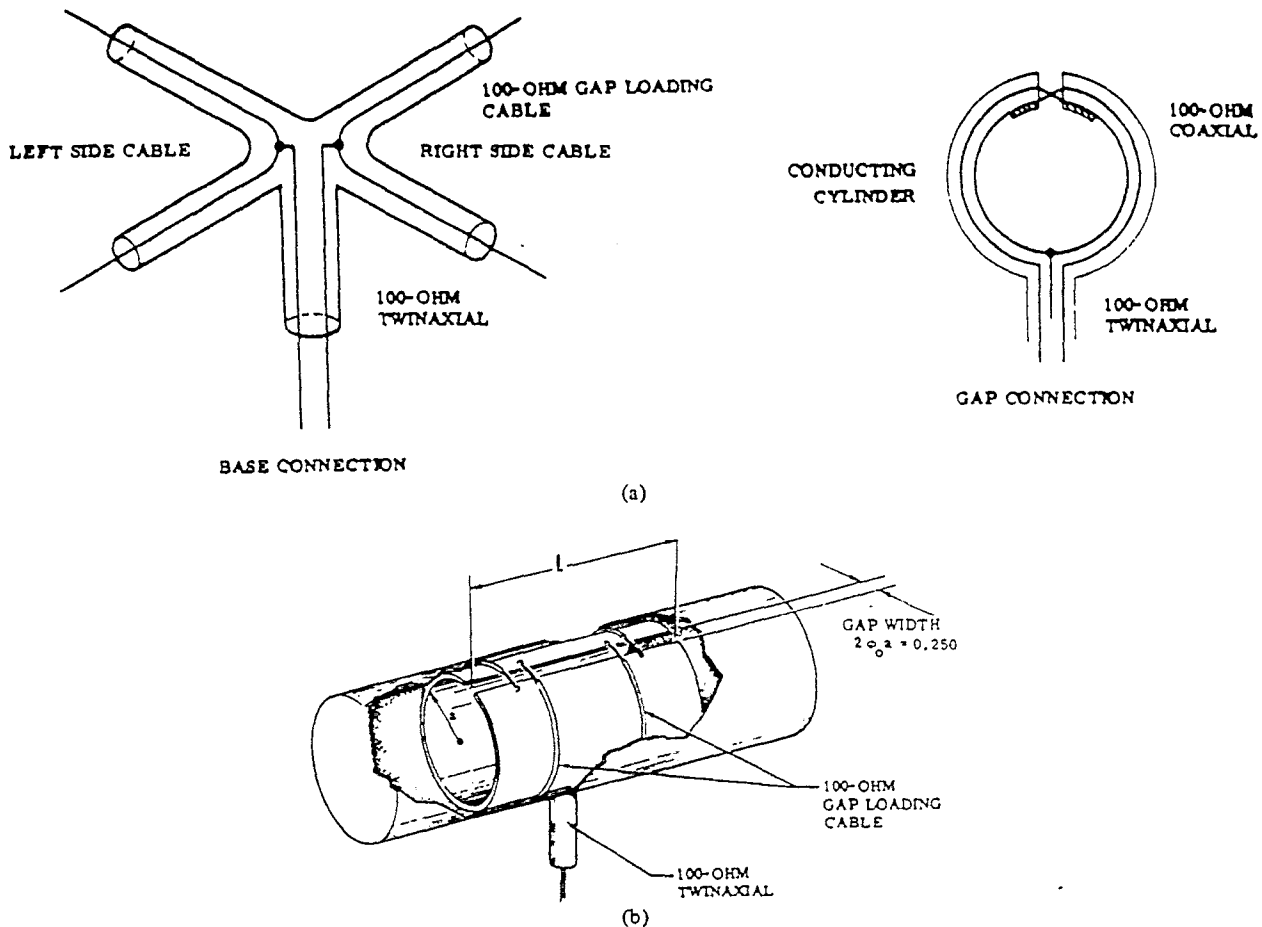
Fig. 16.   Cylindrical moebius loop sensor CML-2B(R). (a) Electrical connections (b) Typical loop configuration.

[31]. These sensors are designed to be part of a specific structure in a way that they will not appreciably affect the current flow on that structure.

1) *Outside Moebius Mutual Inductance (OMM):* Fig. 17 shows three OMM-1A I-dot sensors assembled into a cylindrical antenna [71], [81]. Surface current flowing along the cylinder axis must pass through the sensor's internal cavity. The changing magnetic field produced within the sensor cavity produces a voltage across the gap according to $(1/N)M \, dI/dt$ where M is determined by (12). The signal is taken from the gap by four 100-Ω cables in the same manner as shown in Fig. 16 for the CML sensor. The signal cables are routed to the inside of the sensor for electrical purposes and radiation shielding. The sensor interior and gap are encapsulated with an epoxy material in much the same way as with the CML B-dot sensor. The sensor cables are made of aluminum and teflon (low atomic number) to reduce radiation induced emission of electrons. The differential signal from each sensor is transmitted by cables of equal length positioned to maintain equal and minimum exposure to nuclear radiation. The OMM-1A has a mutual inductance of 2×10^{-9} H and a 10-90 rise time < 0.5 ns. It is 6.4 cm long and of a diameter for use with a 10-cm pipe (outside diameter). A much smaller OMM-2 sensor has been built to measure current in cable shields, conductors, or structural members. It has a mutual inductance

of 2×10^{-9} H and a rise time of < 0.5 ns. It is 8.9 cm long and designed to use with a 2-cm pipe (outside diameter).

2) *Flush Moebius Mutual Inductance (FMM):* The FMM is a radiation hardened sensor for measuring J_{t_n}-dot (time derivative of total current density component normal to the surface) [20]. A sketch of the FMM-1A is shown in Fig. 18 [79]. It is wired and encapsulated much like the OMM type of sensor. In this case, however, it has an equivalent area to convert the current density to a current besides its mutual inductance. It is important to note that the impedance presented by the gap to currents on the surface is negligibly small for frequencies or times of interest so as to not appreciably distort the electric field in the region surrounded by the potted annular slot. In measuring J_{t_n} on a test surface, the portion leaving the sensor plate must pass over the surface of the sensor cavity. This gives rise to a voltage across the sensor gap expressed by (7) where M is determined by (12) and $A_{t_{eq}}$ is determined by [41]. The voltage is taken from the sensor gap by four equally spaced 100-Ω cables in the manner of the CML B-dot sensor of Fig. 16. Cable passages and connection points are provided in the sensor structure which is machined from aluminum. The sensor cavities and gap are filled with an epoxy as a radiation hardening measure. The epoxy extends up from the gap to provide increased voltage standoff and minimize electron transport across the gap. The FMM-1A is
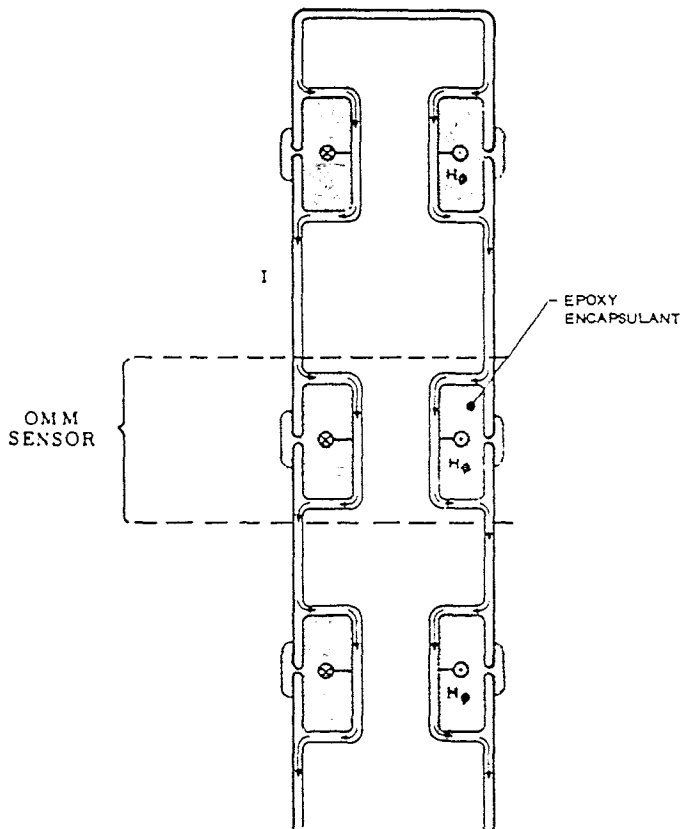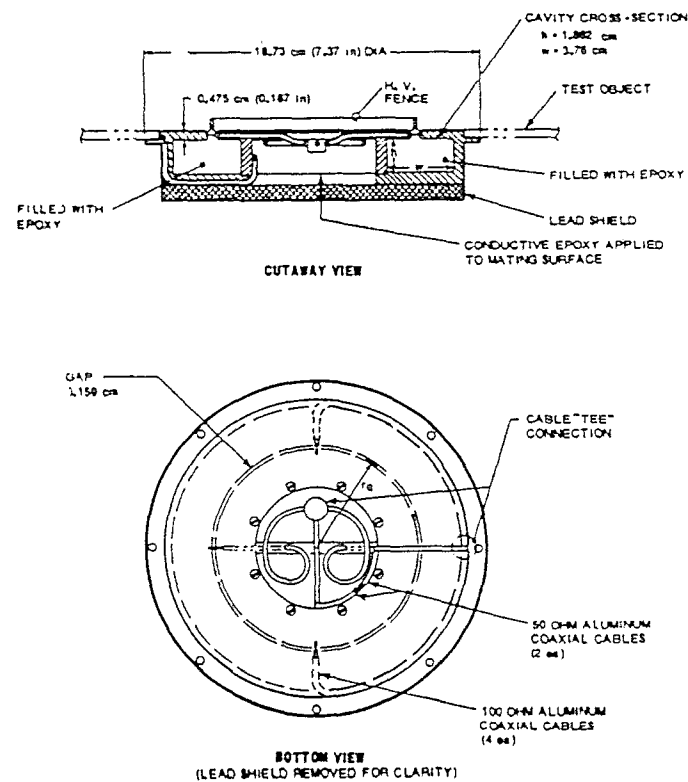
Fig. 17.   Cylindrical antenna with OMM sensors.

CUTAWAY VIEW

BOTTOM VIEW
(LEAD SHIELD REMOVED FOR CLARITY)

Fig. 18.   FMM-1A sensor details.

approximately 19 cm in diameter. It has a mutual inductance of 5×10^{-9} H, an equivalent area of 1×10^{-2} m^2, and a 10-90 rise time < 1 ns.

IV. SUMMARY

Many somewhat optimized sensor designs realized in various specific models have been developed for and employed in transient/broadband electromagnetic measurements, especially for EMP applications. Various details of these sensors will likely be further improved with time and attendent experience.

Various other sensor concepts have been considered, and some will likely be developed in the future [2], [5], [12], [21], [35], [44]. Special passive voltages probes are one likely candidate. Other EMP related sensors such as radiation sensors for γ rays, X rays, and neutrons have also been developed for EMP applications, but such are considered beyond the scope of this paper.

Besides the sensors themselves, one needs to consider various electromagnetic design problems associated with the objects to which the sensor is attached to hold the sensor in a given position and/or transport the resulting signal to the recorder, as well as other adjacent objects [23], [28], [29], [32], [40], [42], [49], [62]-[64].

There has been a vast amount of work on these kinds of electromagnetic sensors. The interested reader is referred to the references for the specifics.

REFERENCES

In the interest of brevity the following abbreviations are used:

SSN   sensor and simulation notes
IN   interaction notes
MN   measurement notes.

These are part of the note series on EMP and related subjects described in "The Compleat Guide to the Notes," INDEX 1-1, February 1973, by Baum. These have played a prominent role in transient/broadband technology. Listings of these can also be found in the *IEEE AP-S Newsletter*. Copies of these papers can be requested from the author, from the Defense Documentation Center, Cameron Station, Alexandria, VA 22314, or from the Editor, Dr. Carl E. Baum, Air Force Weapons Laboratory (NT), Kirtland AFB, NM 871177. In addition, these notes are available at many universities and companies doing research in EMP and electromagnetic theory. Other report numbers used are

AFWL-TR   Air Force Weapons Laboratory Technical Report
           (AFWL-TRs are available from Defense Documenta-
           tion Center, Alexandria, VA 22314.)
AL   Albuquerque Division
           EG&G Inc.
           9733 Coors R., N.W.
           Albuquerque, NM 87114.

[1] R. E. Partridge, "'Invisible' absolute *E*-field probe," SSN 2, Feb. 1964.
[2] —, "Combined *E* and *B*-dot sensor," SSN 3, Feb. 1964.
[3] K. Theobald, "On the properties of loop antennas," SSN 4, Feb. 1964.
[4] C. E. Baum, "Underground testing of close-in EMP sensors," SSN 5, Oct. 1964.
[5] —, "Minimizing transit time effects in sensor cables," SSN 6, Oct. 1964.
[6] —, "Characteristics of the moebius strip loop," SSN 7, Dec. 1964.
[7] —, "Maximizing frequency response of a *B*-dot loop," SSN 8, Dec. 1964.

[8] R. E. Partridge, "Capacitive probe E-field sensors," SSN 11, Feb. 1965.

[9] C. E. Baum, "Electric field and current density measurements in media of constant conductivity," SSN 13, Jan. 1965.

[10] G. L. Fjetland, "Design considerations for a twinaxial cable," SSN 14, Mar. 1965.

[11] C. E. Baum, "Radiation and conductivity constraints on the design of a dipole electric field sensor," SSN 15, Feb. 1965.

[12] L. E. Orsak and A. L. Whitson, "Electric field sensor for EMP simulators'" SSN 18, Dec. 1965.

[13] C. E. Baum, "Combining voltage or current dividers with sensor cables," SSN 19, Nov. 1965.

[14] —, "A technique for the distribution of signal inputs to loops," SSN 23, July 1966.

[15] —, "A technique for measuring electric fields associated with internal EMP," SSN 24, Aug. 1966.

[16] —, "The multiple moebius strip loop," SSN 25, Aug. 1966.

[17] —, "The influence of finite soil and water conductivity on close-in surface electric field measurements," SSN 26, Sept. 1966.

[18] —, "The influence of radiation and conductivity on B-dot loop design," SSN 29, Oct. 1966.

[19] —, "The single-gap cylindrical loop in nonconducting and conducting media," SSN 30, Jan. 1967.

[20] —, "Two types of vertical current density sensors," SSN 33, Feb. 1967.

[21] R. S. Hebbert and L. J. Schwee, "Thin film magnetoresistance magnetometer," SSN 34, Feb. 1967.

[22] C. E. Baum, "Parameters for some electrically-small electromagnetic sensors," SSN 38, Mar. 1967.

[23] —, "Some electromagnetic considerations for a sea-water-based platform for electromagnetic sensors," SSN 39, Mar. 1967.

[24] —, "Conducting shields for electrically-small cylindrical loops," SSN 40, May 1967.

[25] —, "The multi-gap cylindrical loop in nonconducting media," SSN 41, May 1967.

[26] —, "A conical-transmission-line gap for a cylindrical loop," SSN 42, May 1967.

[27] —, "Some considerations for electrically-small multi-turn cylindrical loops," SSN 43, May 1967.

[28] R. W. Sassman, R. W. Latham, and A. G. Berger, "Electromagnetic scattering from a conducting post," SSN 45, June 1967.

[29] R. W. Latham and K. S. H. Lee, "Minimization of induced currents by impedance loading," SSN 51, Apr. 1968.

[30] C. E. Baum, "Some electromagnetic considerations for a rocket platform for electromagnetic sensors," SSN 56, June 1968.

[31] —, "Some considerations for inductive current sensors," SSN 59, July 1968.

[32] R. W. Sassman, R. W. Latham and K. S. H. Lee, "A numerical study on minimization of induced currents by impedance loading," SSN 61, Aug. 1968.

[33] C. E. Baum, "An equivalent-charge method for defining geometries of dipole antennas," SSN 72, Jan. 1969.

[34] —, "Parameters for electrically-small loops and dipoles expressed in terms of current and charge distributions," SSN 74, Jan. 1969.

[35] —, "Electrically-small cylindrical loops for measuring the magnetic field perpendicular to the cylinder axis," SSN 78, Mar. 1969.

[36] —, "The circular parallel-plate dipole," SSN 80, Mar. 1969.

[37] —, "Some further considerations for the circular parallel plate dipole," SSN 86, June 1969.

[38] —, "The single-gap hollow spherical dipole in nonconducting media," SSN 91, July 1969.

[39] —, "The circular flush-plate dipole in a conducting plane and located in nonconducting media," SSN 98, Feb. 1970.

[40] R. W. Latham, and K. S. H. Lee, "Magnetic-field distortion by a specific axisymmetric semi-infinite, perfectly conducting body," SSN 102, Apr. 1970.

[41] —, "Capacitance and equivalent area of a disk in a circular aperture," SSN 106, May 1970.

[42] C. E. Baum, "Two approaches to the measurement of pulsed electromagnetic fields incident on the surface of the earth," SSN 109, June 1970.

[43] R. W. Latham and K. S. H. Lee, "Capacitance and equivalent area of a spherical dipole sensor," SSN 113, July 1970.

[44] C. J. Hall, "The asymmetric dipole as a transient field probe," SSN 115, Aug. 1970.

[45] L. Marin, "Scattering by two perfectly conducting, circular coaxial disks," SSN 126, Mar. 1971.

[46] C. E. Baum, "Further considerations for multi-turn cylindrical loops," SSN 127, Mar. 1971.

[47] K. S. H. Lee and R. W. Latham, "Inductance and current density of a cylindrical shell," SSN 130, June 1971.

[48] F. M. Tesche, "Optimum spacing of N loops in a B-dot sensor," SSN 133, July 1971.

[49] S. W. Lee, V. Jamnejad and R. Mittra, "Near field of scattering by a hollow semi-finite cylinder and its application to EMP studies," SSN 149, May 1972.

[50] P. H. Duncan, Jr., "Analysis of the moebius loop magnetic field sensor," SSN 183, Sept. 1973.

[51] K. S. H. Lee, "Electrically-small ellipsoidal antennas," SSN 193, Feb. 1974.

[52] C. E. Baum, "A figure of merit for transit-time-limited time-derivative electromagnetic field sensors," SSN 212, Dec. 1975.

[53] —, "Electromagnetic pulse interaction close to nuclear bursts and associated EMP environment specification," IN 76, July 1971.

[54] "Some design considerations for signal transmission lines for use with sensors in a nuclear radiation environment," MN 17, Oct. 1973.

[55] H. Whiteside and R. W. P. King, "The loop antenna as a probe," IEEE Trans. Antennas Propagat., pp. 291-297, May 1964.

[56] A. H. Libbey et al., "Development of hardened magnetic field sensors," AFWL-TR-69-58, (vol. I and II), June 1969.

[57] R. Morey et al., "Development and production of multi-gap loop (MGL) series EMP B-dot sensors," AFWL-TR-70-153, Feb. 1971.

[58] J. K. Travers and J. H. Kraemer, "Development and construction of electric field and D-dot sensors," AFWL-TR-70-154, Mar. 1971.

[59] W. R. Edgel, "Hollow spherical dipole D-dot sensor (HSD-4) development," AFWL-TR-75-77, Jan. 1975 (also AL-1147, Jan. 1975).

[60] S. L. Olsen, "Asymptotic conical dipole D-dot sensor development," AFWL-TR-75-263, Jan. 1976 (also AL-1185, Sept. 1975).

[61] T. Summers, "I-dot sensor design and fabrication," AL-516, Nov. 1970.

[62] R. Christiansen and T. Summers, "EMP sensor application guide," AL-524, Dec. 1970.

[63] M. Bumgardner, "Noise associated with the differential E-field sensors," AL-592, June 1971.

[64] W. Motil and M. Bumgardner, "A technique for evaluating measurements obtained from HSD-sensors," AL-647, Oct. 71.

[65] W. Edgel, "I-dot sensor design and fabrication Phase II," AL-678, Dec. 1971.

[66] J. Harrison, "Fabrication and testing of a multi-turn B-dot sensor," AL-735, Feb. 1972.

[67] W. Edgel, "I-dot sensor development," AL-921, June 1973.

[68] —, "B-dot sensor development," AL-952, July 1973.

[69] S. Olsen, "Flush plate dipole D-dot sensor development," AL-1100, Aug. 1974.

[70] W. Edgel, "MGL-6 B-dot sensor development," AL-1101, Aug. 1974.

[71] —, "Radiation hardened I-dot sensor (OMM-1A) for use in Baum antenna," AL-1102, Aug. 1974.

[72] —, "Conforming flat D-dot sensor development," AL-1103, Aug. 1974.

[73] —, "MGL-S7A B-dot sensor development," AL-1104, Aug. 1974.

[74] —, " MTL-2 B-dot sensor development," AL-1105, Aug. 1974.

[75] —, "A small, radiation hardened B-dot sensor (CML-4A)," AL-1106, Aug. 1974.

[76] S. Olsen, "Sensor MGL-8B sensor DW," AL-1186, Sept. 1975.

[77] —, "MGL-S8 B-dot sensor development," AL-1187, Sept. 1975.

[78] G. D. Sower et al., "Cylindrical moebius loop radiation hardened B-dot sensor (CML-6A(R) development," AL-1224, June 1976.

[79] —, et al., "Flush moebius mutual inductance radiation hardened J_n-dot sensor (FMM-1A) development," AL-1226, June 1976.

[80] —, et al., "Cylindrical moebius loop radiation hardened *B*-dot sensor (CML-X3A(R) and CML-X5A(R)) development," AL-1229, June 1976.

[81] —, "Ouside moebius mutual radiation hardened *I*-dot sensor (OMM-2A) development," AL-1232, June 1976.

[82] —, "Parallel mesh dipole radiation hardened *E*-field sensors (PMD-1C) development," AL-1233, June 1976.

[83] B. C. Tupper et al., "EMP instrumentation development," final report, SRI Project 7990, Stanford Research Institute, Menlo Park, CA, June 1972.

[84] C. E. Baum, Ed., "Electromagnetic pulse sensor handbook," EMP Measurement 1-1, June 1971 (original issue).

[85] —, "Electromagnetic pulse instrumentation handbook," EMP Measurement 2-1, June 1971 (original issue).